HHS Public Access

Author manuscript

Brain Behav Immun. Author manuscript; available in PMC 2023 June 02.

Published in final edited form as:

Brain Behav Immun. 2022 January ; 99: 383–396. doi:10.1016/j.bbi.2021.10.010.

IL-1 reprogramming of adult neural stem cells limits neurocognitive recovery after viral encephalitis by maintaining a proinflammatory state

Allison L. Soung[a,b], **Veronica A. Davé**[a,b], **Charise Garber**[a,b], **Eric D. Tycksen**[c], **Lauren L. Vollmer**[a,b], **Robyn S. Klein**[a,b,d,e,*]

[a]Center for Neuroimmunology & Neuroinfectious Diseases, Washington University School of Medicine, St Louis, MO 63110, United States

[b]Department of Medicine, Washington University School of Medicine, St. Louis, MO 63110, United States

[c]McDonnell Genome Institute, Washington University School of Medicine, St Louis, MO 63110, United States

[d]Department of Pathology and Immunology, Washington University School of Medicine, St. Louis, MO 63110, United States

[e]Department of Neuroscience, Washington University School of Medicine, St. Louis, MO 63110, United States

Abstract

Innate immune responses to emerging RNA viruses are increasingly recognized as having significant contributions to neurologic sequelae, especially memory disorders. Using a recovery model of West Nile virus (WNV) encephalitis, we show that, while macrophages deliver the antiviral and anti-neurogenic cytokine IL-1β during acute infection; viral recovery is associated with continued astrocyte inflammasome-mediated production of inflammatory levels of IL-1β, which is maintained by hippocampal astrogenesis via IL-1R1 signaling in neural stem cells (NSC). Accordingly, aberrant astrogenesis is prevented in the absence of IL-1 signaling in NSC, indicating that only newly generated astrocytes exert neurotoxic effects, preventing synapse repair and promoting spatial learning deficits. *Ex vivo* evaluation of IL-1β-treated adult hippocampal NSC revealed the upregulation of developmental differentiation pathways that derail adult neurogenesis in favor of astrogenesis, following viral infection. We conclude that NSC-specific IL-1 signaling

*Corresponding author at: Center for Neuroimmunology & Neuroinfectious Diseases, Washington University School of Medicine, St. Louis, MO 63110, United States; Department of Medicine, Washington University School of Medicine, St. Louis, MO 63110, United States. rklein@wustl.edu (R.S. Klein).

Contributions

A.L.S. and R.S.K. designed the experiments. A.L.S., V.A.D., C.G., and L.L.V. performed experiments. A.L.S., V.A.D., R.S.K., and E.D.T. analyzed the data. A.L.S. and R.S.K. wrote the paper. All authors read and edited the manuscript.

Declaration of Competing Interest

The authors declare that they have no known competing financial interests or personal relationships that could have appeared to influence the work reported in this paper.

Appendix A. Supplementary data

Supplementary data to this article can be found online at https://doi.org/10.1016/j.bbi.2021.10.010.

within the hippocampus during viral encephalitis prevents synapse recovery and promotes spatial learning defects via altered fates of NSC progeny that maintain inflammation.

Keywords

Astrogenesis; Adult neural stem cell; Interleukin-1; Flavivirus encephalitis; Post-infectious cognitive dysfunction; Spatial learning; Synapse elimination

Innate immune molecules modulate a variety of central nervous system (CNS) functions throughout life. These include the maintenance of blood–brain barrier (BBB) function (Jang, 2012), synaptic networks (Filiano, 2016), microglial physiology (Butovsky and Weiner, 2018; Yeh and Ikezu, 2019), astrogenesis, and glial-mediated synapse remodeling (Kanski et al., 2014; Vainchtein, 2018) and repair (Amor et al., 2010; Healy et al., 2020). Within the normal brain, tonic levels of cytokines are expressed by resident cells, including perivascular myeloid and ependymal cells, microglia, astrocytes, oligodendrocytes, and neurons (del Rey et al., 2013; Dixon-Salazar, 2014; Ejlerskov et al., 2015; Michelucci, 2016; Peferoen et al., 2014). During aging, increased expression of cytokines is associated with decreased hippocampal neurogenesis, which is critical for the formation of new memories (Baruch, 2014). Even higher levels of cytokines occur within the CNS during infection with RNA viruses, which is among the risk factors for diseases of pathological forgetting in non-elder adults. RNA viruses may be associated with acute neuroinfectious diseases and may target neurons, astrocytes, and/or neural stem cells (NSC) (Salimi et al., 2016; Tang, 2016). However, the mechanisms responsible for memory disorders in patients who survive neuroinvasive infections are not well understood. Here we find that CNS infection with West Nile virus (WNV), a neurotropic flavivirus, induces persistent memory dysfunction in surviving individuals via direct effects on gene programs in NSC.

Mosquito-borne infections within the *Flaviviridae* family, including West Nile (WNV), Japanese encephalitis (JEV), and Zika (ZIKV) viruses, can cause acute neuroinfectious diseases after neuroinvasion via retrograde transport along neurons or by crossing the BBB within exosomes (Zhou et al., 2018). Flavivirus infections are also associated with chronic complications in adult and adolescent survivors of acute encephalitis, including long-term cognitive impairment, motor deficits, and immune neuropathies (van den Pol, 2009). WNV, which emerged in North America in 1999 and is the leading cause of domestically acquired arboviral disease in the United States (Weaver and Reisen, 2010), specifically targets mature neurons and can induce neuronal cell death, microglial activation, and mononuclear immune cell infiltration, which are recapitulated in animal models (Nagata, 2004). Studies evaluating memory impairments in patients previously diagnosed with WNV neuroinvasive disease (WNND) using cognitive assessment tools report that >50% exhibit significant defects in memory recall and spatial learning that persist and worsen for years after recovery from acute infection (Berg et al., 2010; Sejvar, 2008; Hoffman and Paschal, 2013). Given that these mechanisms may be generalizable to multiple diseases of cognition, and that there are no treatments that reverse memory deficits, there is a pressing need to define the mechanisms that limit cognitive recovery after viral infections.

The formation and consolidation of new memories occurs primarily within the hippocampus and relies on the integrity of trisynaptic circuits between the entorhinal cortex, hippocampal dentate gyrus (DG), and Cornu Ammonis (CA) (Zemla and Basu, 2017). Spatial learning, in particular, relies on the link between synapses within the CA3 region and rates of adult neurogenesis, which occurs via generation of new neurons from NSC within the subgranular zone (SGZ) of the DG (Trouche et al., 2009). Neuroblasts derived from NSC divide, differentiate into neurons, and integrate into existing circuits (Suh et al., 2009), supporting normal memory formation and forgetting (Trouche et al., 2009). Murine behavioral studies altering adult neurogenesis via irradiation or ablation have provided substantial evidence for the role of newborn neurons in hippocampal spatial learning and memory consolidation (Ziv, 2006; Snyder et al., 2005). Reductions in SGZ neurogenesis or increased CA3 synapse elimination in adults impairs spatial memory formation and is associated with a variety of neurodegenerative diseases (Deng et al., 2010; Moreno and Mallucci, 2010; Rola, 2004), and with post-infectious cognitive dysfunction during recovery from WNV and ZIKV encephalitides (Weaver and Reisen, 2010; Davis, 2006).

In this study, we identify a critical role for NSC in the maintenance of proinflammatory levels of IL-1β, which promotes and maintains post-infectious neurocognitive dysfunction. Using an established model of recovery from WNND, we show that, while infiltrating macrophages deliver IL-1β during the acute viral encephalitis period, inflammasome activation in astrocytes results in the continued production of the anti-neurogenic cytokine, interleukin (IL)-1β at proinflammatory levels. Further, we demonstrate that *in vivo* IL-1R1 signaling in NSC is required for the generation of IL-1β-expressing astrocytes, which continues to regulate fate of progeny towards gliogenesis, preventing synapse recovery, and promoting persistent spatial learning and memory deficits in WNV-recovered mice. $Nestin^{Cre+ERT}Il\text{-}1r1^{fl/fl}$ mice, which exhibit NSC-specific deletion of IL-1R1, exhibit restored neurogenesis, repair of CA3 synapses, and improved neural activity with normal spatial learning abilities, compared with littermate controls. Conditional deletion of IL-1R1 in NSC also prevents astrogenesis and astrocyte production of IL-1β, indicating that proinflammatory astrocytes that arise during WNV encephalitis differentiate from newborn glioblasts. Finally, *in vitro* treatment of adult hippocampal NSC with murine IL-1β revealed that developmental neuronal differentiation pathways are utilized to influence adult neurogenesis and astrogenesis after viral infection. These results suggest that IL-1 signaling via NSC prevents synapse recovery required for restoration of spatial learning via alteration in the fates of NSC progeny.

1. Results

1.1. NLRP3 inflammasome contributes to IL-1β production during WNV recovery.

We previously showed that spatial learning defects in WNV-recovered mice are driven by complement- and microglia-mediated elimination of presynaptic termini within the CA3 and IL-1R1-mediated decrease in SGZ neurogenesis (Vasek et al., 2016; Garber, 2018), which both persist long after viral clearance within the CNS. Further analysis determined that hippocampal reactive astrocytes become the predominant source of anti-neurogenic

cytokines after viral clearance, suggesting a critical role for reactive, proinflammatory astrocytes in persistent neurological sequalae (Garber, 2018).

In macrophages, IL-1β is generated via proteolytic cleavage of pro-IL-1 β by Caspase-1 during inflammasome activation, followed by caspase-1-dependent cell lysis, a process termed pyroptosis (Martinon et al., 2002). Transcriptional profiling of hippocampi derived from WNV-recovered animals that exhibit poor spatial learning exhibit higher levels of Caspase-1, but not IL-1α (Garber, 2018), suggesting inflammasome activation in astrocytes leads to generation of IL-1 β. During acute infection of WNV, IL-1 is initially delivered to the virally infected CNS via infiltrating macrophages (Durrant et al., 2013), which do not persist in high numbers during recovery (Garber, 2018). In addition, compared to astrocytes, microglia express negligible levels of IL-1 βin WNV-recovered animals (Garber, 2018). Indeed, detection of activated Caspase-1 in hippocampal ACSA-2^+ astrocytes and $CD11b^+$ microglia/macrophages isolated via magnetic cell sorting from mock- and WNV-infected animals revealed a shift in highest levels from myeloid cells to astrocytes during recovery. Thus, at 7 days post-infection (dpi), when viral loads are highest in the brain (Vasek et al., 2016), Caspase-1 activity is significantly elevated in both ACSA-2^+ and $CD11b^+$ cells isolated from WNV-infected animals compared to those isolated from mock-infected, with significantly greater activation of Caspase-1 activity observed in $CD11b^+$ myeloid cells versus ACSA-2^+ cells (Fig. 1A, top panel). At 25 dpi, however, long after CNS viral clearance (Vasek et al., 2016), the level of activated Caspase-1 was significantly increased in ACSA-2^+ astrocytes isolated from WNV-infected animals compared to mock-infected animals (Fig. 1aA, bottom panel). At this time-point, levels of activated Caspase-1 in $CD11b^+$ myeloid cells isolated from WNV-infected animals were not different from mock-infected animals, confirming the astrocytic specificity of proinflammatory levels of IL-1β production during viral recovery (Fig. 1A, bottom panel). These findings also suggest that IL-1β production by astrocytes involves caspase 1 activity in response to WNV infection.

To further evaluate the potential contribution of inflammasome activation during WNV recovery, we analyzed sequencing data of hippocampal RNA from mock- versus WNV-infected mice at 25 dpi. The data set revealed significant upregulation of the expression of 736 transcripts with subsequent analysis identifying genes associated with the inflammasome complex. These include *Pycard*, which encodes apoptosis-associated speck-like protein containing CARD, *Aim2*, which encodes interferon-inducible protein Aim2, *Casp1*, which encodes caspase-1 precursor, and *Nlrp3*, which encodes NLR family pyrin domain containing 3 (Fig. 1B). PYCARD is an inflammasome adapter protein that is required for the formation of AIM2 and NLRP3 inflammasomes (Martinon et al., 2002).

Next we examined the protein expression levels of particular inflammasome components in hippocampal astrocytes. In a model of sterile, toxin-mediated demyelination, Freeman et al. demonstrated *in vivo* expression of NLRP3 and NLRP4 by activated astrocytes, which demonstrated similar *in vitro* specificities for inflammasome activation as bone-marrow derived macrophages (Freeman, 2017). Analysis of the hippocampal CA3 region of WNV-infected wildtype mice at 7, 25 and 52 dpi revealed an increase in Caspase-1+ GFAP+ and NLRP3+ GFAP+ astrocytes (Fig. 1C,D). Taken altogether, these data indicate that astrocyte

NLRP3 inflammasome-mediated production of IL-1β maintains its elevated levels in the WNV-recovered CNS.

1.2. Nestin^{CreERT}+Il1r1$^{fl/fl}$ animals resist alterations in adult neurogenesis during WNV infection

Given the reported effects of IL-1β on NSC in neuronal proliferation and differentiation during development (Zhang et al., 2013), we generated animals in which we could control the expression of the IL-1 receptor, IL-1R1, in a temporal and cell-type specific manner using a tamoxifen inducible cre expressed under the Nestin promotor. Mitosis in nestin$^+$ NSC gives rise to transit amplifying cells, which differentiate into neuroblasts or glioblasts. Thus, astrocytes may be generated de novo or as a result of astrogliosis. Since astrocyte reactivity during gliosis is associated with increased genetic expression of nestin, we administered tamoxifen one week prior to intracranial (i.c.) infection of *Nestin*$^{CreERT-}$*Il1r1*$^{fl/fl}$ (referred to as Cre$^-$ hereafter) and *Nestin-*$^{CreERT+}$*Il1r1*$^{fl/fl}$ (referred to as Cre$^+$ hereafter) littermates, that latter of which exhibit deletion of IL-1R1 from nestin + cells, but avoids deletion of IL-1R1 from other cell types in response to infection (Tamagno and Schiffer, 2006). Detection of IL-1R1 mRNA within nestin mRNA+ cells via double-label mRNA *in situ* hybridization revelealed loss of receptor from NSC only in Cre$^+$ animals (Supplementary Fig. 1). Of note, since the *Nestin*^{CreERT}-inducible transgenic mouse was generated using 5.8 kb of the nestin promoter and exons 1–3 of the nestin gene (Lagace, 2007); Cre$^+$ animals also exhibited more pronounced detection of nestin RNA than those that were Cre$^-$ (Supplementary Fig. 1). As astrocytes, microglia, and neurons all express IL1-R1, and the direct or indirect role of IL-1β on neurogenesis remains unknown, we also crossed *Il1r1*$^{fl/fl}$ mice with relevant tamoxifen inducible cre lines, including *Cx*$_3$*cr1*^{CreERT} (microglia), *Aldh1l1*^{CreERT} (astrocytes), and *Camk2*^{CreERT} (excitatory neurons). *Aldh1l1*^{CreERT}*Il1r1*$^{fl/fl}$ and *Camk2*^{CreERT}*Il1r1*$^{fl/fl}$ mice received tamoxifen one week prior to infection. *Cx*$_3$*cr1*^{CreERT}*Il1r1*$^{fl/fl}$ animals were administered tamoxifen two weeks prior to infection to allow CX*3*CR1 expressing peripheral myeloid cells to recover IL-1R1 expression, so that only microglia remain deficient (Goldmann, 2016). Monitoring of all Cre$^-$ and Cre$^+$ animals from each inducible cre line infected with WNV for daily weight loss did not show any significant differences between mock- and WNV-infected animals in any of the cre line groups (Supplementary Fig. 2). Importantly, qRT-PCR analysis of Prominin-1$^+$ NSCs collected from the hippocampus of mock- and WNV-infected Cre$^-$ and Cre$^+$ (nestin) animals revealed an increase of IL-1R1 mRNA expression in WNV-infected Cre$^-$ animals compared to mock-infected but not in Cre$^+$ animals (Supplementary Fig. 3A). Furthermore, *in situ* detection of WNV mRNA in wildtype, Cre$^-$ and Cre$^+$ (nestin) animals revealed similar viral levels within the cortical and hippocampal regions of the CNS (Supplementary Fig. 3B). Together these data validate the deletion of the IL-1 receptor from NSCs and indicate that loss of IL-1R1 during acute WNV infection did not significantly impact peak disease parameters.

In addition to being an intermediate filament protein and a known NSC marker, nestin is expressed on endothelial cells of the CNS (Suzuki et al., 2010). During WNV infection, IL-1β also acts on both endothelial cells and perivascular astrocytes, contributing to their activation and destabilizing the blood–brain barrier (BBB) (Daniels et al., 2014), the latter

of which increases neuroinvasion of WNV (Miner, 2015). Acute BBB permeability, as measured by IgG intensity, in the hippocampus of WNV-infected Cre^- and Cre^+ (nestin) animals were similarly increased compared to mock-infected animals (Supplementary Fig. 3C), as were increases of $Iba1^+$ expressing cells, compared to mock-infected animals at 7 dpi. As previously shown in WT mice (Vasek et al., 2016), elevated $Iba1^+$ expression in the hippocampus of both WNV-infected Cre^- and Cre^+ (nestin) animals persisted throughout recovery (Supplementary Fig. 4A-C). Elevated Iba1+ expression within the hippocampus is present at 25 dpi in all inducible cre lines, suggesting that disrupted IL-1 signaling in distinct cell types does not alter microglia activation (Supplementary Fig. 4D-F).

To determine whether WNV-mediated reduction of neurogenesis requires IL-1 signaling, in NSC, we administered BrdU to Cre^- and Cre^+ (nestin) mice and evaluated the number of proliferating hippocampal neuronal progenitor cells, which express doublecortin (DCX+) by immunohistochemistry (Supplementary Fig. 3D, Fig. 2A). While WNV-recovered, Cre^- mice exhibited the expected reduction of SGZ BrdU-labeled neuroblasts, Cre^+ animals exhibited normal levels of neuroblast proliferation at both 7 and 25 dpi (Supplementary Fig. 3E, Fig. 2B). As confirmation that alternations in neuroblast proliferation are specific to IL-1 signaling in NSC, we examined BrdU-labeled neuroblasts of WNV-recovered animals in our other inducible cre lines. When IL-1 signaling in disrupted in microglia, astrocytes, or excitatory neurons, neuroblast proliferation is reduced to similar rates compared to Cre^- animals (Supplementary Fig. 5). Similarly, pulse-chase BrdU studies, evaluating the generation of newly born neurons at 45 dpi (Fig. 2C) revealed a reduction of BrdU+ NeuN+ (mature neurons) in WNV-recovered Cre^-, but not in Cre^+ mice with deletion specific to nestin + cells (Fig. 2D). These data support the notion that IL-1 signaling specifically in NSC underlies derailment of adult neurogenesis during WNV encephalitis and recovery.

1.3. NSC IL-1R1 signaling promotes the generation of proinflammatory astrocytes.

To further investigate the role of IL-1R1 signaling in the fate of NSC, we determined whether more glial progenitor cells were produced versus neural progenitor cells within the hippocampal DG via detection of BrdU within $Sox9^+$ proliferating astroblasts (Supplementary Fig. 3D, Fig. 3A). Significantly higher numbers of $BrdU^+Sox9^+$ astroblasts at both 7 and 25 dpi were detected in WNV-infected Cre^-, but not Cre^+, animals, indicative of IL-1R1-mediated regulation of NSC progeny towards an astrocyte fate. Notably, in the absence of NSC IL-1R1 signaling, Cre^+ WNV-infected animals did not undergo a substantial increase in proliferating astrocytes (Supplementary Fig. 3G, Fig. 3B), suggesting increases in reactive astrocyte numbers occur as a result of astrogenesis. To further confirm this, we administered BrdU to mice during the peak of WNV encephalitis and then evaluated the number of newly generated astrocytes within the hippocampal DG. WNV-infected Cre^- animals exhibited an increase in BrdU-labeled Sox9-expressing astrocytes at 52 dpi within the DG. In contrast, WNV-infected Cre^+ mice exhibited no increase in newly generated astrocytes during recovery from WNV encephalitis (Fig. 3C,D).

As shown previously (Garber, 2018), $IBA1^+$ macrophages remain the primary source of IL-1β during acute infection despite the deletion of IL-1 signaling in NSC (Supplementary Fig. 3H). Also, astrocyte production of IL-1β during acute infection remains unchanged

between mock- and WNV-infected Cre$^-$ and Cre$^+$ animals (Supplementary Fig. 3I). During recovery, however, infection with WNV leads to an increase of GFAP + astrocytes, which persist in the hippocampal parenchyma for at least a month after viral clearance and become the main source of IL-1β (Garber, 2018). Analysis of the hippocampal CA3 region of WNV-recovered Cre$^-$ mice at both 25 and 52 dpi confirmed that astrocytes remain the source of IL-1β in the recovering CNS. However, WNV-recovered Cre$^+$ mice exhibit a reduction the production by IL-1β by reactive astrocytes (Fig. 3E,F). Accordingly, detection of caspase-1 protein was reduced in Cre+ relative to Cre$^-$ mice (Supplementary Fig. 6). These data suggest that the early increase in IL-β production by reactive astrocytes occurs as a result of astrogenesis, which continue to express IL-1β when macrophages are no longer present in the hippocampus.

1.4. NSC-specific deletion of IL-1R1 improves presynaptic termini recovery.

We previously showed that WNV-recovered animals exhibit specific loss of synapses within the CA3 region of the hippocampus (Vasek et al., 2016). Given that *Nestin-Cre^{ERT+}xIL1R1$^{fl/fl}$* mice were protected from derailed neurogenesis and that hippocampal synapse recovery is observed in *Il1r1$^{-/-}$* mice (Garber, 2018), we examined recovery of synapses within the CA3 of WNV-recovered *Nestin-Cre^{ERT+}xIL1R1$^{fl/fl}$* mice. Quantitative 3D assessment of volumes of colocalized presynaptic (synaptophysin$^+$) and postsynaptic (homer1$^+$) puncta within the hippocampal CA3 region of WNV-infected mice revealed significantly decreased synaptic boutons in Cre$^-$ animals at 52 dpi compared to Cre$^+$ animals and mock-infected controls (Supplementary Videos 1,2). The decrease in colocalization was due to a reduction in synaptophysin$^+$ presynaptic terminal volume, with no change in homer$^+$ postsynaptic terminals (Fig. 4A). Of note, synaptophysin$^+$ debris in the hippocampus was present as well. Consistent with this, WNV-infected Cre$^-$ and Cre$^+$ animals exhibited acute loss of synaptophysin$^+$ presynaptic terminals at 7 dpi (Supplementary Fig. 3F), with WNV-infected Cre$^-$ animals continuing to show decreased numbers of synaptophysin$^+$ presynaptic terminals at 25 and 52 dpi. In contrast, WNV-infected Cre$^+$ animals displayed recovery of synaptophysin$^+$ presynaptic terminals at both 25 and 52 dpi (Fig. 4B,C). Despite the cell-specific loss of IL-1R1 signaling in microglia, astrocytes and excitatory neurons results, these WNV-infected Cre$^+$ animals display similar elimination of synaptophysin$^+$ presynaptic terminals as Cre$^-$ littermates (Supplementary Fig. 7). These data support the notion that IL-1 specifically targets NSC, which leads to limited repair of eliminated synapses within the hippocampal CA3 of WNV-recovered mice.

1.5. Nestin$^{CreERT+}$Il1r1$^{fl/fl}$ mice exhibit normal spatial learning

Adult neurogenesis and synaptic plasticity are critical for spatial learning. To examine spatial learning and memory, animals were assessed for their ability to spatially locate and remember the location of a target hole over the course of 5 days using the Barnes maze paradigm. Behavioral testing at 45 dpi, a time-point at which we previously showed spatial learning deficits in WNV-recovered wildtype mice (Vasek et al., 2016) (Fig. 5A), revealed that Cre$^+$ animals were significantly protected from spatial learning deficits (Fig. 5B) compared to Cre$^-$ animals. Area under the curve analysis for each mouse, which depicts the performance of individual animals within each group across all 5 days of testing, demonstrated that WNV-recovered Cre$^-$ mice exhibited significantly higher errors

than those of mock-infected or WNV-infected Cre$^+$ animals (Fig. 5C). To assess differences in exploratory behavior that might affect performance in the Barnes maze task, we also performed open field testing (OFT) one day prior to Barnes maze testing. The distance travelled and average speed within 5 min of testing were similar for mock- and WNV-infected mice of all genotypes, indicating that motor deficits do not underlie spatial learning defects in WNV-recovered Cre$^-$ mice (Fig. 5D,E). Additionally, loss of IL-1R1 in NSC did not result in differences between groups in the time spent in the center (Fig. 5F), which assesses anxiety. These studies demonstrate a critical role for NSC IL-1R1 signaling in limiting cognitive recovery after WNV encephalitis.

1.6. IL-1R1 signaling in NSC is associated with reduced neural activity in WNV-infected animals

The formation of memories involves an increase in the strength of a relatively small number of synapses that connect neurons into a circuit (Bailey et al., 2015). Because of the enduring nature of memory formation, it is thought that gene expression is involved in the process. The immediate early gene c-fos encodes a transcription factor and has long been known as a molecular marker of neural activity. The neuron's activity is transformed into intracellular calcium influx through NMDA receptors and L-type voltage sensitive calcium channels (Rajadhyaksha, 1999). *C-fos* upregulation has also been shown to correlate with spatial and behavior learning and memory in mice (Gallo et al., 2018).

Given the repair of synapses observed in WNV-recovered Nestin $^{CreERT+}Il1r1^{fl/fl}$ mice, we tested whether IL-1R1 signaling in NSC impacts neural activity. Mock- and WNV-infected animals underwent two days of Barnes maze training; one day of habituation where animals are introduced to the environment and one day of acquisition where animals learn to find the location of the target box (Fig. 6A) (Gawel et al., 2019). Following the animals' first attempt to learn the target hole's location, CNS tissue was harvest and assessed for neural activity, or C-FOS+ cells. Analysis of C-FOS+ cells throughout the hippocampus, including the DG, CA3 region (Fig. 6B,C), and entorhinal cortex, revealed a significant reduction in neural activity in WNV-recovered Cre$^-$ mice. In contrast, WNV-infected Cre$^+$ animals displayed recovery of neural activity throughout the hippocampus (Fig. 6D). These data demonstrate that IL-1R1 signaling limits recovery of neural activity after recovery from viral encephalitis.

1.7. IL-1β-mediated regulation of neurogenesis and astrogenesis harnesses developmental signaling pathways in adult NSC

Previous *in vitro* studies have shown IL-1β reduces embryonic NSC proliferation and enhances gliosis (Borsini et al., 2015), while separate *in vivo* studies using IL-1β overexpression mice show decreases in neurogenesis and synaptic plasticity (Ryan et al., 2013). However, few studies have focused on the mechanism in which IL-1R1 regulates NSC fate in the adult hippocampus. To identify genes and pathways downstream of IL-1R1 signaling, murine NSC derived from the adult hippocampus were treated for 3 days with 100 ng/mL of murine IL-1β (acute experiments) (Borsini, 2017), 7 days with 10 ng/mL of murine IL-1β (chronic experiments) (Zonis et al., 2015), or left untreated, followed by RNA-sequencing. RNA analyses revealed 4142 transcripts in acutely treated NSC and

409 differentially expressed transcripts in chronically treated NSC (Fig. 7A, Supplementary Tables 1-4). In both IL-1β-treated groups, pathway analysis identified signatures associated with several immune pathways, including interferon gamma signaling, IL-6-Jak-STAT3 signaling, and tumor necrosis factor alpha signaling via NF-κB (Supplementary Fig. 8 and Suplementary Tables 5-6). Enrichment of the IL-6-Jak-STAT3 signaling pathway in both treatment groups (Fig. 7B) implied a possible activation of astrogenesis, given that several genes in this pathway promote astrocyte differentiation. These include *Stat3*, which when translocated to the nucleus induces expression of astrocytic genes (He, 2005), and *Il6* and *Socs1*, regulators/activators of *Stat3* (Fig. 7C) (Leu et al., 2003; Mallette et al., 2010). To validate activation of the IL-6-Jak-STAT3 pathway in Cre+ and Cre− animals, we detected phosphorylated STAT3 (phospho-STAT3) by immunostaining at 7 dpi. We found that phospho-STAT3-positive nuclei were more common in the SGZ of the DG of Cre− mice than Cre+ mice (Fig. 7C), supporting our *ex vivo* finding that IL-1β may promote STAT3 signaling and subsequent astrogenesis among NSCs of mice infected with WNV.

2. Discussion

IL-1 is generally known as a cytokine that, at peak inflammation levels, stimulates myeloid cells to amplify inflammation. In the brain, proinflammatory levels of IL-1 also stimulate astrocytes to express leukocyte chemoattaracts and thereby amplify inflammation. Here, we show that proinflammatory levels of IL-1β also regulate NSC progeny fate in a manner that maintains an inflammatory state via the generation of astrocytes that express high levels of IL-1β. In our study, we found that infiltrating myeloid cells are the primary source of activated caspase-1 during acute viral infection, however, newly generated astrocytes are a source of similar levels of caspase-1 leading to production of the anti-neurogenic cytokine, IL-1β, that continuously signals via NSC to promote astrogenesis, rather than neurogenesis, maintaining synapse loss in the CA3 region, decreased neural activity, and spatial learning defects. These data indicate that IL-1 signaling via NSC not only negatively influences neural correlates of memory but also contributes to neuro-inflammation. Modulating this “gliogenic switch” in the adult hippocampus was thus identified as a potential strategy to resist viral-mediated cognitive dysfunction.

In previous studies, we demonstrated that IL-1 exerts critical roles in regulating antiviral effector T cell responses that clear virus (Durrant et al., 2013; Ramos, 2012). IL-1β, a member of the IL-1 signaling family, requires cleavage by caspase-1 during inflammasome activation (Martinon et al., 2002). Inflammasome complexes are composed of multiple proteins, including an NLR, an adaptor apoptosis-associated speck-like protein containing a CARD (ASC) domain that contains a caspase activation and recruitment domain (CARD) domain or a pyrin domain (PYD), and the effector protein caspase-1. Currently, several members of the NLR family have been identified, with NLRP3 being the most well-studied of the family. Studies have shown that the NLRP3 inflammasome is activated by viral RNA, including WNV. The NLRP3 inflammasome and IL-1β signaling is required for limiting WNV associated disease within the CNS. Mice lacking NLRP3 or its downstream effector capase-1 displayed increased susceptibility and clinical disease in response to WNV infection (Ramos, 2012). However, WNV does not directly target astrocytes. Other mechanisms of inflammasome activation in astrocytes could include potassium efflux out of

the cell, the generation of reactive oxygen species (ROS), the translocation of NLRP3 to the mitochondria, and the release of cathepsins into the cytosol after lysosomal destabilization (Vanaja et al., 2015). While our studies identify the NLRP3 inflammasome as a contributor to astrocytic IL-1β production, further studies focusing on the mechanisms of activating the astrocyte inflammasome during neuronotropic viral infections are warranted.

IL-1 is also a well-known and a potent inhibitor of NSC proliferation. The overexpression of IL-1 has been associated with several neurodegenerative diseases, such as Alzheimer's disease and Parkinson's disease (Nuzzo, 2014; Monson, 2014), supporting the hypothesis that neuroinflammatory changes are an important component to diseases of pathological forgetting. Direct inoculation of the hippocampus with IL-1 leads to a decrease in neurogenesis (Hueston, 2018; Liu et al., 2019), while the use of the IL-1R antagonist (IL-1Ra) (Ben Menachem-Zidon et al., 2008), administration of the anti-IL-1R1 drug anakinra (Garber, 2018), or genetic deletion of IL-1R1 (Wu, 2012) can inhibit the anti-neurogenic actions of IL-1. IL-1 mediated inhibition of neurogenesis is proposed through two mechanisms: 1) inhibition of NSC proliferation, and 2) alteration of cell fate of NSC. In support of the first mechanism, studies have described the role of IL-1 in decreasing the incorporation of thymidine analogues in NSC (Garber, 2018; Liu et al., 2019) as well as the number of immature neurons (Hueston, 2018; Liu et al., 2019). IL-1 effects on cell fate have been demonstrated through *in vitro* studies where the stimulation of NSC with IL-1α and IL-1β cause an increase in the number of astroglia-like cells and a decrease in differentiated neurons (Zhang et al., 2013; Ajmone-Cat et al., 2010). In our model of WNV recovery, IL-1 directly acts on NSC to increase astrogenesis and decrease neurogenesis, which had not been confirmed *in vivo* or in other diseases of pathological forgetting. While this is detrimental for learning and memory, the "gliogenic switch' may be an adaptive mechanism to limit the numbers of viral targets, given the specific neuronal tropism of WNV.

During WNV infection synapse loss is mediated by the expression of classical complement proteins on microglia (Vasek et al., 2016). Here we demonstrate that NSC-specific deletion of IL-1R1 improves WNV-mediated synapse recovery. However, the elimination of synapses may also be advantageous for the prevention of subsequent neuron infection and/or transsynaptic viral spread. Indeed, spread of WNV has been observed within peripheral and central neurons (Maximova et al., 2016; Samuel et al., 2007). Several other neurotrophic virus, such as Rabies virus, Herpes Simplex virus (HSV) types 1 and 2, and vesicular stomatitis virus, are known to transsynaptically spread in CNS neurons (Ugolini, 2011; Beier, 2013). Specifically, HSV-1 produces glycoprotein C, a protein known to bind and antagonize complement C3 (Friedman et al., 1984). This may allow the virus to travel through neurons undetected. These data suggest that synapse loss may play a protective, rather than a pathogenic role in West Nile virus infections to prevent viral spread.

Prior research has suggested activated microglia as key players in directing astrogenesis (Liddelow et al., 2017). In our own WNV model, we demonstrated that the loss of IFNγ signaling leads to the attenuation of astrocyte activation during recovery from infection. This effect is most likely secondary to the lack of microglia activation, given that the specific deletion of *Ifngr* in microglia was sufficient to promote synapse recovery and protect against spatial learning deficits (Garber, 2018). Similarly, the activation of the

inflammasome complex within myeloid cells has been implicated in IL-1β production with IL-1 targeting multiple cell types including neural precursor cells (Lamkanfi and Dixit, 2014; Wang, 2007). However, many of these results are context dependent and the ontogeny of reactive astrocytes, specifically during both acute viral encephalitis and recovery, and regulation of their expression of anti-neurogenic cytokines are unknown. In prior studies, using transcriptional profiling and pathway analyses of hippocampal tissues from WNV-recovered animals, we detected increased expression of anti-neurogenic and decreased expression of pro-neurogenic factors (Vasek et al., 2016; Garber, 2018). Consistent with this, pulse-labeling using BrdU incorporation revealed a significant increase in reactive astrocytes as the predominant source of anti-neurogenic cytokines including IL-1β at the expense of the generation of new neurons within the hippocampus. Here, we determined via cell-specific deletion in multiple cell types, including neurons, astrocytes, microglia, and NSC, that rescue of aberrant astrogenesis and repair of lost synapses is accomplished only via IL-1R1 deletion in NSC.

In response to injury, reactive astrocytes were previously thought to migrate to the injury sites. Live imaging studies, however, demonstrate that this is not always the case. Instead, astrocytes remain in their tiled-domain and become hypertrophic (Wilhelmsson, 2006). Neither proliferation nor the migration of differentiated astrocytes contribute to the total increase of GFAP+ cells observed at injury sites, leading to a new focus on identifying other sources of adult astrocytes. Currently researchers have identified multiple other sources, such as radial glial, NSC within the subventricular zone and subgranular zone, and NG2+ cells. We found that NSC are a cellular origin for reactive astrocyte in a viral infection model.

This study also indicates that endogenous NSC might be harnessed for CNS repair. NSC fates may be manipulated towards the generation of differentiating neuroblasts, which can be directed towards sites of injury sites via administration of localizing cues. This may be achieved by chemokine-directed migration, such as CXCL12, towards injury sites. CXCL12 and its receptor CXCR4 that is predominately expressed on NSC are essential for modulating NSC survival, proliferation, and migration (Williams et al., 2014; Li et al., 2011). Recent data demonstrate the CXCR7, another receptor for CXCL12, has important roles in cell cycle regulation and proliferation of NSC (Abe et al., 2018; Wang, 2016). The genetic knockdown of CXCL12 or CXCR7 led to a decrease number of proliferating cells and DCX + neuroblasts in adult mice, ultimately leading to learning and memory deficits (Trousse, 2019). Future studies are needed to investigate the translational potential of our finding in enhancing adult neurogenesis to counter cognitive dysfunction associated with neurological disorders.

Along with IL-1, a variety of inflammatory molecules have been studied for their ability to induce a reactive phenotype *in vitro* (Liddelow et al., 2017) and *in vivo* (Shinozaki, 2017). The functional outcomes of these newly generated astrocytes and their contributions to neuro-inflammation and neuropathology have been significantly debated over the past several years. Important studies have described roles of glial cells in providing neurotrophic support to injured neurons and contributing to circuitry remodeling around lesion sites (Sofroniew, 2015). Other studies have highlighted detrimental and inhibitory outcomes of

gliosis, including the amplification of inflammation and inhibition of neuronal repair (Silver et al., 2015). Reactive astrocytes that adopt neurotoxic or neurotrophic phenotypes can be distinguished by distinct genetic signatures (Liddelow et al., 2017). IL-1α, TNF, and C1q, in particular, has been shown to promote neurotoxic, reactive astrocytes *in vitro* (Liddelow et al., 2017). Our model of WNV recovery also exhibits elevated production of IL-1, TNF, and C1q (Vasek et al., 2016). We also observed the *in vivo* development and persistence of astrocytes with panreactive and neurotoxic markers, including Gpb2 (Garber, 2018); an interferon (IFN)-inducible guanylate-binding protein that drives inflammasome activation during infectious diseases (MacMicking, 2012). Thus, lack of recovery of synapses in our model may be due to the generation of this subset of reactive astrocytes or, alternatively, to the loss of a specific astrocyte population that normally promotes synapto-genesis (John Lin, 2017). Further studies are needed to phenotypically identify astrocyte subpopulations that are effectors or regulators of inflammation, and whether these astrocytes are distinct from those that foster, sustain and eliminate synapses in the course of life.

3. Methods

3.1. Animals

8–10 weeks old male and female mice were used for all experiment. *Il1r1*$^{fl/fl}$, *Nestin*^{CreERT2}, *Cx3cr1*^{CreERT2}, *Aldh1l1*^{CreERT2}, and *Camk2*^{CreERT2} mice were obtain from Jackson Laboratories. Transgenic animals were backcrossed more than ten generations to C57BL/6 mice at Jackson Laboratories. All experiments followed the guidelines approved by the Washington University School of Medicine Animals Safety Committee (protocol no. 20170064).

3.2. Mouse models of WNV infection

M. Diamond at Washington University in St Louis provided the WNV-NS5-E218A strain utilized for intracranial infections. WNV-NS5-E218A harbors a single point mutation in the gene encoding 2′-*O*-methyl-transferase. Deeply anesthetized mice were administered 1×10^4 plaque-forming units (p.f.u.) of WNV-NS5-E218A in 10 μL of 0.5% fetal bovine serum in Hank's balanced salt solution (HBBS) into the third ventricle of the brain with a guided 29-guage needle. Mock-infected mice were intracranially injected with 10 μL of 0.5% in HBSS into the third ventricle of the brain with a guided 29-guage needle.

3.3. Mouse neural stem cells

Primary hippocampal NSC were obtained from C57BL6 mice at 7–8 weeks of ages. Dissociated cells were cultured at a density of $2x10^5$ cells/mL in proliferation media, consisting of DMEM (Gibco), 0.2% herparin (Stem Cell), 1x B27 supplement (Gibco), 20 ng/mL mouse EGF (Stem Cell), 20 ng/mL mouse bFGF (Stem Cell), penicillin/streptomycin (Gibco), and L-glutamine (Gibco). Neurospheres were allowed to grow with medium changes every other day. For neural expansions on an adherent monolayer, neurospheres were dissociated with Accutase and plated on Matrigel (Corning)-coated plates. Media was changed every other day.

3.4. In vitro IL-1β treatments

All samples, including untreated, were cultured in proliferation media for 7 days. For treatment conditions, recombinant murine IL-1β was added to cultures at doses of either 10 ng/mL for all 7 days (for chronic experiments) or 100 ng/mL for the last 3 days of the experiment (for acute experiments). All cultures were terminated on the same day and RNA was collected for sequencing. Doses were chosen based on previous literature (Zonis et al., 2015; Green, 2012).

3.5. In vivo bromodeoxyuridine (BrdU) labeling

BrdU (Sigma Aldrich) in sterile PBS was injected intraperitoneally for all experiments. For acute and short-term recovery immunohistochemical timepoints (harvested at 7 or 25 dpi), mice were given 100 mg/kg of BrdU at 24 and 48 h before tissue harvest. For neuronal and astrocyte BrdU labelling (harvested at 52 dpi), mice were given 50 mg/kg every 12 h beginning at 3 dpi and ending at 7 dpi, for a total of seven doses.

3.6. Immunohistochemistry

Mice were anesthetized and perfused with ice-cold Dulbecco's PBS (Gibco) followed by ice-cold 4% paraformaldehyde (PFA). Brains were then immersion-fixed overnight in 4% PFA followed by cryoprotection in three exchanges of 30% sucrose for 72 h, then frozen in OCT compound (Fischer). For phospho-STAT3 detection, antigen retrieval was performed before staining by boiling in saline-sodium citrate buffer for 15 min. 10-μm-thick fixed-frozen coronal tissue sections were washed with PBS and permeabilized with 0.1% Triton X-100 (Sigma-Aldrich). Nonspecific antibodies were blocked with 5–10% normal goat or donkey serum (Sigma Aldrich) at room temperature for 1 h. Slides were incubated in 1 N of HCl (Sigma Aldrich) at 45 °C for 30 min, followed by 0.05 M sodium borate (Sigma Aldrich) washes, in order to denature DNA when detecting BrdU. Slides were then incubated in primary antibody (identified below) or isotype-matched IgG overnight at 4 °C. Following washes in PBS, slides were then incubated in secondary antibodies at room temperature for 1 h. Nuclei were then counterstained with DAPI (Invitrogen) and coverslips with ProLong Gold Antifade Mountant (Thermo Fisher). Immunofluorescent images were acquired using a Zeiss LSM 880 confocal laser scanning microscope and processed using software (Zeiss). Immunofluorescent signals were quantified by an individual blind to sample identify using the public domain NIH Image analysis software, ImageJ.

3.7. Antibodies for immunohistochemistry

The following primary antibodies were used for IHC analyses: NeuN (1:1000; Cell Signaling, cat no. 12943S, clone D3S3I), BrdU (1:250; Abcam, cat. no. ab1893, polyclonal), doublecortin (1:125; Cell Signaling, cat. no. 4604S, polyclonal), GFAP (1:250; Thermo, cat. no. 13–0300, clone 2.2B10), IL-1β (1:100; R&D, cat. no. AF-401, polyclonal), IBA1 (1:500; Synaptic Systems, cat. no. 234006, polyclonal), Homer (1:200; Synaptic Systems, cat. no. 160002, polycloncal), Sox9 (1:500; Millipore, cat no. AB5535, polyclonal), c-Fos (1:1000; Millipore, cat. no. ABE457, polyclonal), Caspase-1 (1:200, Cell Signaling, cat. no. 24232S, monoclonal), NLRP3 (1:200, R&D Systems, cat. no. MAB7578, monoclonal), synaptophysin (1:250; Synaptic Systems, cat. no. 101004, polyclonal), and phospho-STAT3

(1:100, Abcam, cat. no. ab76315, monoclonal). Secondary antibodies conjugated to Alexa-488, Alexa-555, or Alexa-647 (Invitrogen, polyclonal) were used at a 1:500 dilution.

3.8. In situ hybridization

Mice were sacrificed and brains were dissected and sectioned onto slides as described for immunohistochemistry. Detection of *Nestin* and *Il1r1* RNA was performed with RNAscope probes and RNAscope 2.5HD Duplex Assay (Advanced Cell Diagnostics), following the manufacturer's protocols. Briefly, after probe hybridization, amplification, and detection, tissues were stained with 50% hematoxylin, submersed in 0.02% ammonia water, rinsed, submersed in xylene, and mounted in Permount (Fisher Scientific). Slides were imaged on an AxioImager Z2 microscope (Zeiss) at 40x magnification.

3.9. 3D reconstruction of confocal z-stack images

Confocal z-stacks images were taken using a Zeiss LSM 880 laser scanning microscope, consisting of at least 5 images. Volocity 3D image software was used to transform images into three-dimensional reconstruction videos.

3.10. Behavioral testing

Open field testing (OFT) and Barnes maze testing were performed as previously described. In brief, each mouse received two trials per day over the course of five consecutive days. For each trial, mice were given 3 min to explore the Barnes maze platform and to find the target hole. If a mouse did not find the target hole within the test period, it was gently guided in the hole. At the end of a trial, the mice remained in the target hole for 1 min before being placed back into their home cage between trials. The number of errors (or number of nose pokes over non-target holes) was recorded. Prior to Barnes maze testing, animals were tested via OFT to monitor differences in exploratory behavior. Each mouse was given 5 min to explore an empty arena before being placed back into its home cage. Both the Barnes maze platform and the open-field arena were decontaminated with 70% ethanol between trials and/or mice. All trials were video recorded and scored by ANY-maze software.

4. Ex vivo isolation of neural stem cells, microglia, and astrocytes with microbeads

Mice were anesthetized and intracardially perfused with ice-cold dPBS (Gibco). Brains were removed, minced and enzymatically digested in collagenase D (Sigma, 50 mg/ml), TLCK trypsin inhibitor (Sigma, 100 μg/ml), DNase I (Sigma, 100 U/μl), HEPES, pH 7.2 (Gibco, 1 M) all in HBSS (Gibco) for 1 h at 37 °C with shaking. Tissue was triturated and spun down at 300 g for 10 min. Cells were washed with MACS buffer. Myelin$^+$ (Miltenyi Biotec, Cat 130-096-733), Prominin-1$^+$ neural stem cells (Miltenyi Biotec, Cat 130-092-333), ACSA-2$^+$ astrocytes (Miltenyi Biotec, Cat 130-097-678), CD11b$^+$ microglia (Miltenyi Biotec, Cat 130-049-601) were removed or isolated using manual MACS according to the manufacturer's instructions.

4.1. RNA sequencing and bioinformatics

Total RNA was isolated from mock- and WNV-infected hippocampi as well as non-treated and treated NSC using the RNA Plus Mini Kit (Qiagen) according to the manufacturer's instructions. The amount of total RNA extracted was measured on a Nanodrop 2000 spectrophotometer and quality of purified RNA was assessed using an Agilent Bioanalyzer. Ribosomal RNA was removed by an RNase-H method using RiboErase kits (Kapa Biosystems). mRNA was then fragmented in reverse transcriptase buffer and heating to 94° for 8 min. mRNA was reverse transcribed to yield cDNA using Superscript III RT enzyme (Life Technologies, per manufacturer's instructions) and random hexamers. A second strand reaction was performed to yield ds-cDNA. cDNA was then blunt ended, had an A base added to the 3′ ends, and then had Illumina sequencing adapters ligated to the ends. Ligated fragments were then amplified for 12–15 cycles using primers incorporating unique dual index tags. Fragments were sequenced on an Illumina NovaSeq-6000 using paired end 150 base pair reads. Basecalls and demultiplexing were performed with Illumina's bcl2fastq2 software and the reads were then aligned to the Ensembl release 76 primary assembly with STAR version 2.5.1a and gene counts were derived with Subread:featureCount version 1.4.6-p5. All gene counts were then imported into the R/Bioconductor package EdgeR and TMM normalization size factors were calculated to adjust for differences in library size. Ribosomal genes and genes not expressed in at least three samples greater than one count-per-million were excluded from further analysis. The TMM size factors and the matrix of counts were then imported into the R/Bioconductor package Limma with the voomWithQualityWeights function. Differential expression analysis was then performed to analyze for differences between treatments and the results were filtered for only those genes with Benjamini-Hochberg false-discovery rate (FDR) adjusted p-values ≤ 0.05. For each treatment comparison with Limma, global perturbations in known MSigDb gene sets were assessed using the R/Bioconductor package GAGE to test for changes in expression of the reported log 2 fold-changes reported by Limma in each term versus the background log 2 fold-changes of all other genes. Only perturbations against background fold-changes with FDR adjusted p-values ≤ 0.05 were considered significant.

4.2. Caspase-1-activity assessment.

Inflammasome formation was assessed using the bioluminescent Caspase-Glo 1inflammasome -assay. Isolated hippocampal astrocytes were plates at 10^5 cells/well in MACS buffer in 96-well plates according the manufacturer's instructions. Briefly, 100 μL Caspase-Glo 1 reagent (containing MG132 inhibitor in the final concentration of 60 μmol/L) or Caspase-Glo 1 YVAD-CHO reagent (containing Ac-YVAD-CHO inhibitor at a final concentration of 1 μmol/L) was added to the 96-well plate containing 100 μL of blank reaction, mock-infected cells, or WNV-infected cells in culture medium. Well contents were gently mixed, and plates were incubated at room temperature for 1 h to allow stabilization of the luminescent signal. Luminescence was recorded using the microplate reader.

4.3. Quantitative RT-PCR

RNA was isolated from *ex-vivo* cells using Qiagen RNeasy kit according to the manufacturer's instructions. RNA was treated with DNAse prior to cDNA synthesis using

random primers and MultiScribe reverse transcriptase (Applied Biosystems) using the following conditions: 25 °C for 10 min, 48 °C for 30 min, and 95 °C for 50 min. qRT-PCR was performed using Universal SYBR green supermix (Bio-Rad), and data are reported as 2^-ddCt.

4.4. Statistical analysis

Statistical analyses and graph generations were performed using Prism 7.0 (GraphPad Software). Unpaired Student's *t*-test or one-way or two-way analysis of variance (ANOVA) with appropriate post-test to correct for multiple comparisons were performed as indicated in the figure legends. A P values of ≤0.05 was considered significant. Sample sizes for behavioral testing experiments were predetermined by the power analysis. For all experiments, animals were randomly assigned to mock WNV infection. Investigators were blinded to group allocation during data collection and analyses.

Supplementary Material

Refer to Web version on PubMed Central for supplementary material.

Acknowledgements

The authors would like to thank W. Beatty at the Molecular Microbiology Imaging facility at Washington University School of Medicine, the Washington University Center for Cellular Imaging (WUCCI), and A. Yoo for critical reading of the manuscript. This work was support by NSF grant DGE-1745038 to A.L.S. and NIH grants R01NS116788, R01NS104471, and R012052632 to R.S.K.

References

Jang JW, et al. , 2012. Melatonin reduced the elevated matrix metalloproteinase-9 level in a rat photothrombotic stroke model. J. Neurol. Sci 323, 221–227. [PubMed: 23046750]

Filiano AJ, et al. , 2016. Unexpected role of interferon-γ in regulating neuronal connectivity and social behavior. Nature 535, 425–429. [PubMed: 27409813]

Butovsky O, Weiner HL, 2018. Microglial signatures and their role in health and disease. Nat. Rev. Neurosci 19 (10), 622–635. [PubMed: 30206328]

Yeh H, Ikezu T, 2019. Transcriptional and epigenetic regulation of microglia in health and disease. Trends Mol. Med 25 (2), 96–111. [PubMed: 30578089]

Kanski R, van Strien ME, van Tijn P, Hoi EM, 2014. A star is born: new insights into the mechanism of astrogenesis. Cell. Mol. Life Sci 71, 433–447. [PubMed: 23907612]

Vainchtein ID, et al. , 2018. Astrocyte-derived interleukin-33 promotes microglial synapse engulfment and neural circuit development. Science (80_.) 359, 1269–1273.

Amor S, Puentes F, Baker D & Valk P Van Der. Inflammation in neurodegenerative diseases. Immunology 129, 154–169 (2018).

Healy LM, Yaqubi M, Ludwin S, Antel JP, 2020. Species differences in immune - mediated CNS tissue injury and repair: a (neuro)inflammatory topic. Glia 68 (4), 811–829. [PubMed: 31724770]

del Rey A, Balschun D, Wetzel W, Randolf A, Besedovsky HO, 2013. A cytokine network involving brain-borne IL-1β, IL-1ra, IL-18, IL-6, and TNFα operates during long-term potentiation and learning. Brain. Behav. Immun 33, 15–23. [PubMed: 23747799]

Dixon-Salazar TJ, et al. , 2014. MHC Class I limits hippocampal synapse density by inhibiting neuronal insulin receptor signaling. J. Neurosci 34, 11844–11856. [PubMed: 25164678]

Ejlerskov P et al. Lack of neuronal IFN-β-IFNAR causes lewy body- and Parkinson's disease-like dementia. Cell 163, 324–339 (2015). [PubMed: 26451483]

Michelucci A, et al. , 2016. The neurogenic potential of astrocytes is regulated by inflammatory signals. Mol. Neurobiol 53, 3724–3739. [PubMed: 26138449]

Peferoen L, Kipp M, van der Valk P, van Noort JM, Amor S Oligodendrocyte-microglia cross-talk in the central nervous system. Immunology 141, 302–313 (2014). [PubMed: 23981039]

Baruch K, et al. , 2014. Aging-induced type I interferon response at the choroid plexus negatively affects brain function. Science (80-) 346, 89–93.

Salimi H, Cain MD, Klein RS, 2016. Encephalitic arboviruses: emergence, clinical presentation, and neuropathogenesis. Neurotherapeutics 13, 514–534. [PubMed: 27220616]

Tang H, et al. , 2016. Zika virus infects human cortical neural precursors and attenuates their growth. Cell Stem Cell 18, 587–590. [PubMed: 26952870]

Zhou J-H, Wang Y-N, Chang Q-Y, Ma P, Hu Y, Cao X, 2018. Type III interferons in viral infection and antiviral immunity. Cell. Physiol. Biochem 51 (1), 173–185. [PubMed: 30439714]

van den Pol AN, 2009. Viral infection leading to brain dysfunction: more prevalent than appreciated? Neuron 64, 17–20. [PubMed: 19840542]

Weaver SC, Reisen WK, 2010. Present and future arboviral threats. Antiviral Res. 85, 328. [PubMed: 19857523]

Nagata N, et al. , 2004. Differential localization of neurons susceptible to enterovirus 71 and poliovirus type 1 in the central nervous system of cynomolgus monkeys after intravenous inoculation. J. Gen. Virol 85, 2981–2989. [PubMed: 15448361]

Berg PJ, Smallfield S, Svien L, 2010. An investigation of depression and fatigue post West Nile virus infection. South Dakota Med. J. South Dakota State Med. Assoc 63 (127–129), 131–133.

Sejvar JJ, et al. , 2008. Neurocognitive and functional outcomes in persons recovering from West Nile virus illness. J. Neuropsychol 2, 477–499. [PubMed: 19824176]

Hoffman J, Paschal K, 2013. Functional Outcomes of Adult Patients With West Nile Virus Admitted to a Rehabilitation Hospital. J. Geriatr. Phys. Ther 36, 55–62. [PubMed: 22785181]

Zemla R, Basu J, 2017. Hippocampal function in rodents. Curr. Opin. Neurobiol 43, 187–197. [PubMed: 28477511]

Trouche S, Bontempi B, Roullet P, Rampon C, 2009. Recruitment of adult-generated neurons into functional hippocampal networks contributes to updating and strengthening of spatial memory. Proc. Natl. Acad. Sci. U. S. A 106, 5919–5924. [PubMed: 19321751]

Suh H, Deng W, Gage FH, 2009. Signaling in adult neurogenesis. Annu. Rev. Cell Dev. Biol 25 (1), 253–275. [PubMed: 19575663]

Ziv Y, et al. , 2006. Immune cells contribute to the maintenance of neurogenesis and spatial learning abilities in adulthood. Nat. Neurosci 9, 268–275. [PubMed: 16415867]

Snyder JS, Hong NS, McDonald RJ, Wojtowicz JM, 2005. A role for adult neurogenesis in spatial long-term memory. Neuroscience 130 (4), 843–852. [PubMed: 15652983]

Deng W, Aimone JB, Gage FH, 2010. New neurons and new memories: How does adult hippocampal neurogenesis affect learning and memory? Nat. Rev. Neurosci 11 (5), 339–350. [PubMed: 20354534]

Moreno JA, Mallucci GR, 2010. Dysfunction and recovery of synapses in prion disease: Implications for neurodegeneration. Biochem. Soc. Trans 38, 482–487. [PubMed: 20298207]

Rola R, et al. , 2004. Radiation-induced impairment of hippocampal neurogenesis is associated with cognitive deficits in young mice. Exp. Neurol 188, 316–330. [PubMed: 15246832]

Davis LE, et al. , 2006. West Nile virus neuroinvasive disease. Ann. Neurol 60, 286–300. [PubMed: 16983682]

Vasek MJ, et al. , 2016. A complement-microglial axis drives synapse loss during virus-induced memory impairment. Nature 534 (7608), 538–543. [PubMed: 27337340]

Garber C, et al. , 2018. Astrocytes decrease adult neurogenesis during virus-induced memory dysfunction via IL-1 article. Nat. Immunol 19, 151–161. [PubMed: 29292385]

Martinon F, Burns K, Tschopp J, 2002. The Inflammasome: A molecular platform triggering activation of inflammatory caspases and processing of proIL-β. Mol. Cell 10, 417–426. [PubMed: 12191486]

Durrant DM, Robinette ML, Klein RS, 2013. IL-1R1 is required for dendritic cell-mediated T cell reactivation within the CNS during west nile virus encephalitis. J. Exp. Med 210, 503–516. [PubMed: 23460727]

Freeman L, et al. , 2017. NLR members NLRC4 and NLRP3 mediate sterile inflammasome activation in microglia and astrocytes. J. Exp. Med 214, 1351–1370. [PubMed: 28404595]

Zhang K, Xu H, Cao L, Li K, Huang Q, 2013. Interleukin-1β inhibits the differentiation of hippocampal neural precursor cells into serotonergic neurons. Brain Res. 1490, 193–201. [PubMed: 23085314]

Tamagno I, Schiffer D, 2006. Nestin expression in reactive astrocytes of human pathology. J. Neurooncol 80, 227–233. [PubMed: 16826367]

Lagace DC, et al. , 2007. Dynamic contribution of nestin-expressing stem cells to adult neurogenesis. J. Neurosci 27, 12623–12629. [PubMed: 18003841]

Goldmann T, et al. , 2016. Origin, fate and dynamics of macrophages at central nervous system interfaces. Nat. Immunol 17, 797–805. [PubMed: 27135602]

Suzuki S, Namiki J, Shibata S, Mastuzaki Y, Okano H, 2010. The neural stem/progenitor cell marker nestin is expressed in proliferative endothelial cells, but not in mature vasculature. J. Histochem. Cytochem 58, 721–730. [PubMed: 20421592]

Daniels BP, Holman DW, Cruz-Orengo L, Jujjavarapu H, Durrant DM, Klein RS, Griffin DE, 2014. Viral pathogen-associated molecular patterns regulate blood-brain barrier integrity via competing innate cytokine signals. MBio 5 (5).

Miner JJ, et al. , 2015. The TAM receptor Mertk protects against neuroinvasive viral infection by maintaining blood-brain barrier integrity. Nat. Med 21, 1464–1472. [PubMed: 26523970]

Bailey CH, Kandel ER, Harris KM, 2015. Structural components of synaptic plasticity and memory consolidation. Cold Spring Harb. Perspect. Biol 7, 1–29.

Rajadhyaksha A, et al. , 1999. L-type Ca2+ channels are essential for glutamate-mediated CREB phosphorylation and c-fos gene expression in striatal neurons. J. Neurosci 19, 6348–6359. [PubMed: 10414964]

Gallo FT, Katche C, Morici JF, Medina JH, Weisstaub NV, 2018. Immediate early genes, memory and psychiatric disorders: focus on c-Fos, Egr1 and Arc. Front. Behav. Neurosci 12.

Gawel K, Gibula E, Marszalek-Grabska M, Filarowska J, Kotlinska JH, 2019. Assessment of spatial learning and memory in the Barnes maze task in rodents—methodological consideration. Naunyn-Schmiedeberg's Arch. Pharmacol 392 (1), 1–18.

Borsini A, Zunszain PA, Thuret S, Pariante CM, 2015. The role of inflammatory cytokines as key modulators of neurogenesis. Trends Neurosci. 38, 145–157. [PubMed: 25579391]

Ryan SM, O'Keeffe GW, O'Connor C, Keeshan K, Nolan YM, 2013. Negative regulation of TLX by IL-1β correlates with an inhibition of adult hippocampal neural precursor cell proliferation. Brain. Behav. Immun 33, 7–13. [PubMed: 23510989]

Borsini A, et al. , 2017. Rescue of IL-lβ-induced reduction of human neurogenesis by omega-3 fatty acids and antidepressants. Brain. Behav. Immun 65, 230–238. [PubMed: 28529072]

Zonis S, Pechnick RN, Ljubimov VA, Mahgerefteh M, Wawrowsky K, Michelsen KS, Chesnokova V, 2015. Chronic intestinal inflammation alters hippocampal neurogenesis. J. Neuroinflammation 12 (1).

He F, et al. , 2005. A positive autoregulatory loop of Jak-STAT signaling controls the onset of astrogliogenesis. Nat. Neurosci 8, 616–625. [PubMed: 15852015]

Leu C-M, Wong F-H, Chang C, Huang S-F, Hu C.-p., 2003. Interleukin-6 acts as an antiapoptotic factor in human esophageal carcinoma cells through the activation of both STAT3 and mitogen-activated protein kinase pathways. Oncogene 22 (49), 7809–7818. [PubMed: 14586407]

Mallette FA, Calabrese V, Ilangumaran S, Ferbeyre G, 2010. SOCS1, a novel interaction partner of p53 controlling oncogeneinduced senescence. Aging (Albany. NY) 2, 445–452. [PubMed: 20622265]

Ramos HJ, et al. , 2012. IL-1β signaling promotes CNS-intrinsic immune control of West Nile virus infection. PLoS Pathog. 8, e1003039. [PubMed: 23209411]

Vanaja SK, Rathinam VAK, Fitzgerald KA, 2015. Mechanisms of inflammasome activation: recent advances and novel insights. Trends Cell Biol. 25, 308–315. [PubMed: 25639489]

Nuzzo D, et al. , 2014. Inflammatory mediators as biomarkers in brain disorders. Inflammation 37, 639–648. [PubMed: 24292800]

Monson NL, et al. , 2014. Elevated CNS inflammation in patients with preclinical Alzheimer's disease. J. Cereb. Blood Flow Metab 34, 30–33. [PubMed: 24149932]

Hueston CM, et al. , 2018. Chronic interleukin-1β in the dorsal hippocampus impairs behavioural pattern separation. Brain. Behav. Immun 74, 252–264. [PubMed: 30217534]

Liu X, Nemeth DP, McKim DB, Zhu L, DiSabato DJ, Berdysz O, Gorantla G, Oliver B, Witcher KG, Wang Y, Negray CE, Vegesna RS, Sheridan JF, Godbout JP, Robson MJ, Blakely RD, Popovich PG, Bilbo SD, Quan N, 2019. Cell-type-specific interleukin 1 receptor 1 signaling in the brain regulates distinct neuroimmune activities. Immunity 50 (2), 317–333.e6. [PubMed: 30683620]

Ben Menachem-Zidon O, Goshen I, Kreisel T, Ben Menahem Y, Reinhartz E, Ben Hur T, Yirmiya R, 2008. Intrahippocampal transplantation of transgenic neural precursor cells overexpressing interleukin-1 receptor antagonist blocks chronic isolation-induced impairment in memory and neurogenesis. Neuropsychopharmacology 33 (9), 2251–2262. [PubMed: 17987063]

Wu MD, et al. , 2012. Adult murine hippocampal neurogenesis is inhibited by sustained IL-1β and not rescued by voluntary running. Brain. Behav. Immun 26, 292–300. [PubMed: 21983279]

Ajmone-Cat MA, Cacci E, Ragazzoni Y, Minghetti L, Biagioni S, 2010. Progliogenic effect of IL-1α in the differentiation of embryonic neural precursor cells in vitro. J. Neurochem 113, 1060–1072. [PubMed: 20236219]

Maximova OA, Bernbaum JG, Pletnev AG, 2016. West nile virus spreads transsynaptically within the pathways of motor control: anatomical and ultrastructural mapping of neuronal virus infection in the primate central nervous system. PLoS Negl. Trop. Dis 10, e0004980. [PubMed: 27617450]

Samuel MA, Wang H, Siddharthan V, Morrey JD, Diamond MS, 2007. Axonal transport mediates West Nile virus entry into the central nervous system and induces acute flaccid paralysis. Proc. Natl. Acad. Sci. U. S. A 104, 17140–17145. [PubMed: 17939996]

Ugolini G, 2011. Rabies virus as a transneuronal tracer of neuronal connections. Adv. Virus Res 79.

Beier KT, et al. , 2013. Transsynaptic tracing with vesicular stomatitis virus reveals novel retinal circuitry. J. Neurosci 33, 35–51. [PubMed: 23283320]

Friedman HM, Cohen GH, Eisenberg RJ, Seidel CA, Cines DB, 1984. Glycoprotein C of herpes simplex virus 1 acts as a receptor for the C3b complement component on infected cells. Nature 309 (5969), 633–635. [PubMed: 6328323]

Liddelow SA, Guttenplan KA, Clarke LE, Bennett FC, Bohlen CJ, Schirmer L, Bennett ML, Münch AE, Chung W-S, Peterson TC, Wilton DK, Frouin A, Napier BA, Panicker N, Kumar M, Buckwalter MS, Rowitch DH, Dawson VL, Dawson TM, Stevens B, Barres BA, 2017. Neurotoxic reactive astrocytes are induced by activated microglia. Nature 541 (7638), 481–487. [PubMed: 28099414]

Lamkanfi M, Dixit V, 2014. Mechanisms and functions of inflammasomes. Cell 157 (5), 1013–1022. [PubMed: 24855941]

Wang X, et al. , 2007. Interleukin-1β mediates proliferation and differentiation of multipotent neural precursor cells through the activation of SAPK/JNK pathway. Mol. Cell. Neurosci 36, 343–354. [PubMed: 17822921]

Wilhelmsson U, et al. , 2006. Redefining the concept of reactive astrocytes as cells that remain within their unique domains upon reaction to injury. Proc. Natl. Acad. Sci. U. S. A 103, 17513–17518. [PubMed: 17090684]

Williams JL, Patel JR, Daniels BP, Klein RS, 2014. Targeting CXCR7/ACKR3 as a therapeutic strategy to promote remyelination in the adult central nervous system. J. Exp. Med 211, 791–799. [PubMed: 24733828]

Li M, Chang CJ, Lathia JD, Wang L.i., Pacenta HL, Cotleur A, Ransohoff RM, 2011. Chemokine receptor CXCR4 signaling modulates the growth factor-induced cell cycle of self-renewing and multipotent neural progenitor cells. Glia 59 (1), 108–118. [PubMed: 21046557]

Abe P, Wust HM, Arnold SJ, van de Pavert SA, Stumm R, 2018. CXCL12-mediated feedback from granule neurons regulates generation and positioning of new neurons in the dentate gyrus. Glia 66 (8), 1566–1576. [PubMed: 29537098]

Wang Y, et al. , 2016. CXCR7 participates in CXCL12-mediated cell cycle and proliferation regulation in mouse neural progenitor cells. Curr. Mol. Med 16, 738–746. [PubMed: 27573194]

Trousse F, et al. , 2019. Knockdown of the CXCL12/CXCR7 chemokine pathway results in learning deficits and neural progenitor maturation impairment in mice. Brain. Behav. Immun 80, 697–710. [PubMed: 31100368]

Shinozaki Y, et al. , 2017. Transformation of astrocytes to a neuroprotective phenotype by microglia via P2Y1 receptor downregulation. Cell Rep. 19, 1151–1164. [PubMed: 28494865]

Soffoniew MV, 2015. Astrogliosis. Cold Spring Harb. Perspect. Biol 7 (2), a020420.

Silver J, Schwab ME, Popovich PG, 2015. Central nervous system regenerative failure: role of oligodendrocytes, astrocytes, and microglia. Cold Spring Harb. Perspect. Biol 7.

MacMieking JD, 2012. Interferon-inducible effector mechanisms in cell-autonomous immunity. Nat. Rev. Immunol 12 (5), 367–382. [PubMed: 22531325]

John Lin CC, et al. , 2017. Identification of diverse astrocyte populations and their malignant analogs. Nat. Neurosci 20, 396–405. [PubMed: 28166219]

Green HF, et al. , 2012. A role for interleukin-1β in determining the lineage fate of embryonic rat hippocampal neural precursor cells. Mol. Cell. Neurosci 49, 311–321. [PubMed: 22270046]

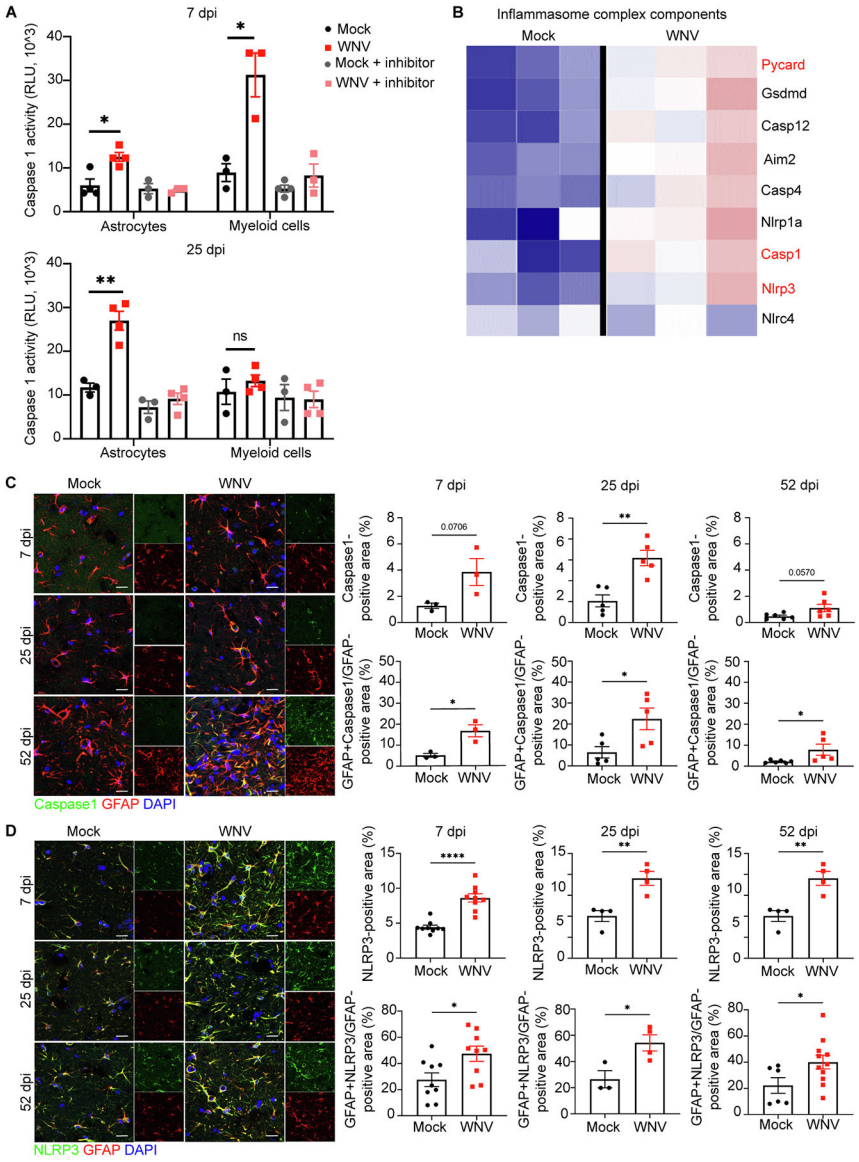

Fig. 1.

NLRP3/Caspase-1 inflammasome complex is involved in IL-1β production by astrocytes. A. Caspase-1 activity assessment in isolated hippocampal astrocytes and microglia at 7 and 25 dpi using Caspase-1® assay; n = 3–4 animals per group. B. Heat map showing relative expression of significantly altered inflammasome complex genes of mock versus WNV-recovered hippocampi at 25 dpi, each column represents an individual mouse. Font red signify most well-studied inflammasome components. C. Representative immunostaining of Caspase-1 (green), GFAP (red) and DAPI (blue) in hippocampal CA3 region of mock or WNV-infected wildtype animals at 7, 25, and 52 dpi, followed by quantification of percent area of Caspase-1 and GFAP + Caspase-1 + area, normalized to the total GFAP + area; n = 3(7), 5 (25, 52). D. Representative immunostaining of NLRP3 (green), GFAP (red) and DAPI (blue) in hippocampal CA3 region of mock or WNV-infected wildtype animals at 7, 25, and 52 dpi, followed by quantification of percent area of NLRP3 and GFAP + NLRP3

+ area, normalized to the total GFAP + area; n = 9 (7dpi), 3–4 (25dpi), 4–11 (52dpi). Data were pooled from at least two independent experiments. Scale bars, 15 μm. Data represent the mean ± s.e.m. and were analyzed by two-way ANOVA and corrected for multiple comparisons.

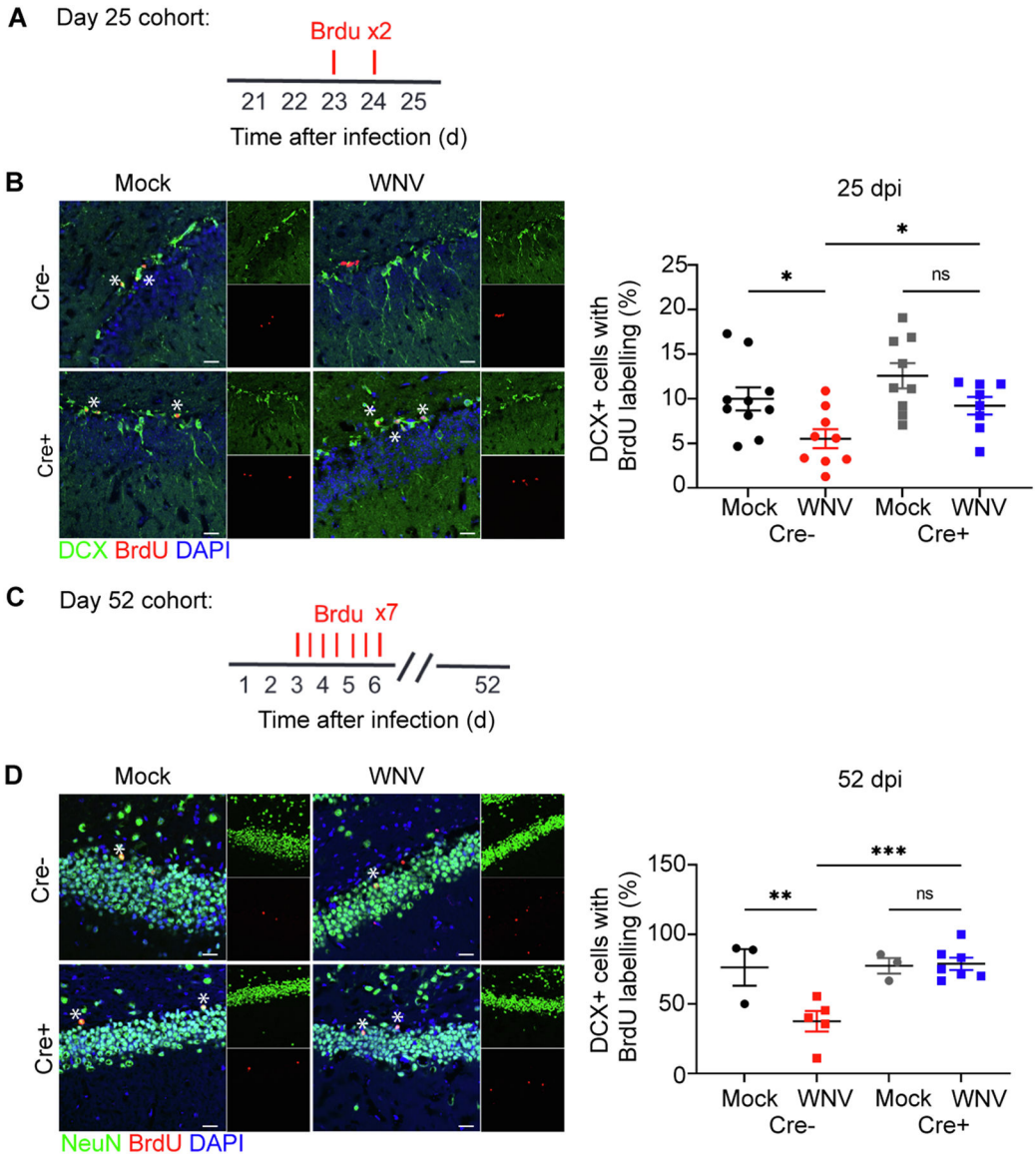

Fig. 2.

Animals deficient in IL1-R1 on NSC resist changes to neurogenesis and astrogenesis during recovery. A. Experimental design: mice were given BrdU (100 mg per kg body weight) by intraperitoneal injection at 24 and 48 h (red lines above) before harvest at 25 dpi B. Microscopy of the dentate gyrus of mock or WNV-infected Cre− or Cre+ animals at 25 dpi, showing staining of BrdU (red), neuroblast (green), and DAPI (blue), followed by quantification of percent BrdU + DCX + cells, normalized to the total number of DCX^+ cells; n = 10 (Mock Cre^-), 9 (WNV Cre^-, Mock Cre^+), 8 (WNV Cre^+). C. Experimental design: mice were given intraperitoneally injected with BrdU (50 mg per kg body weight) every 12 h for 2.5 days (seven injections) beginning at 3 dpi (red lines above) before harvest at 52 dpi. D. Microscopy of the dentate gyrus of mock or WNV-infected Cre− or Cre+ animals at 52 dpi, showing staining of BrdU (red), mature neurons (green), and DAPI (blue), followed by quantification of percent $BrdU^+NeuN^+$ cells, normalized to the total number

of $BrdU^+$ cells; n = 3 (Mock Cre^-, Mock Cre^+), 5 (WNV Cre^-), 7 (WNV Cre^+). Data were pooled from at least two independent experiments. Scale bars, 20 μm. Data represent the mean ± s.e.m. and were analyzed by two-way ANOVA and corrected for multiple comparisons.

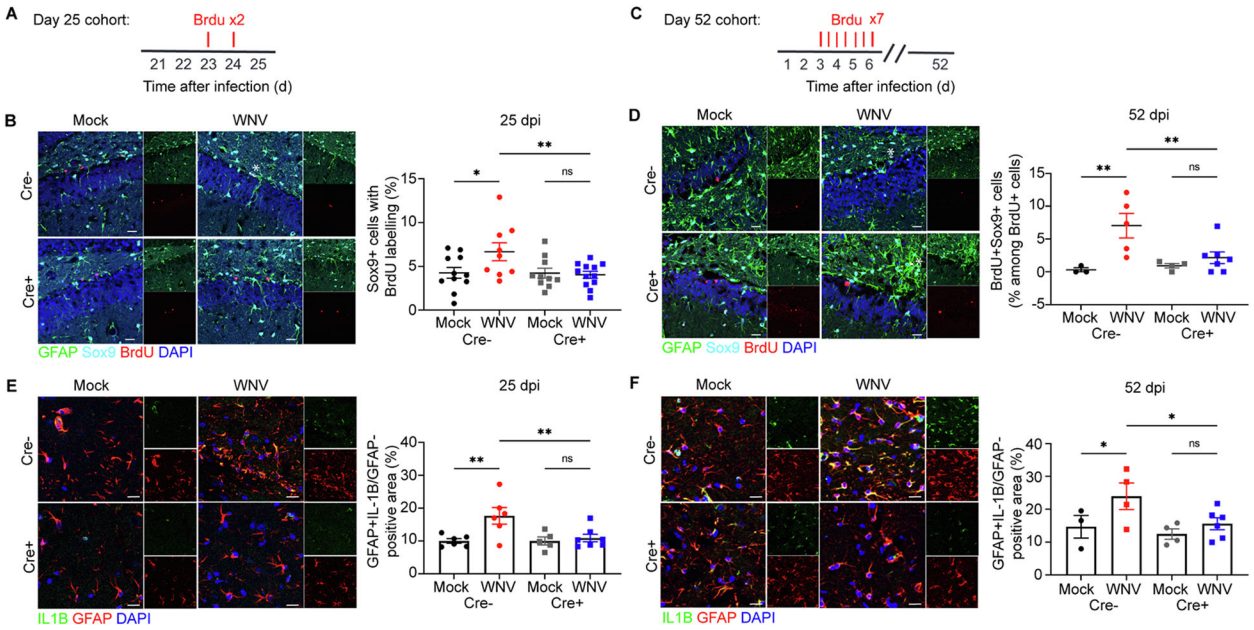

Fig. 3.

Astrogenesis and astrocyte production of IL-1β is attenuated during recovery when IL-1R1 is specifically deleted from NSC. A. Experimental design: mice were given BrdU (100 mg per kg body weight) by intraperitoneal injection at 24 and 48 h (red lines above) before harvest at 25 dpi B. Microscopy of the dentate gyrus of mock or WNV-infected Cre− or Cre+ animals at 25 dpi, showing staining of BrdU (red), astrocytes (green, cyan), and DAPI (blue), followed by quantification of percent BrdU + Sox9 + cells, normalized to the total number of $Sox9^+$ cells; n = 11 (Mock $Cre^−$), 9 (WNV $Cre^−$), 10 (Mock Cre^+), 12 (WNV Cre^+). C. Experimental design: mice were given intraperitoneally injected with BrdU (50 mg per kg body weight) every 12 h for 2.5 days (seven injections) beginning at 3 dpi (red lines above) before harvest at 52 dpi D. Microscopy of the dentate gyrus of mock or WNV-infected Cre− or Cre− animals at 52 dpi, showing staining of BrdU (red), astrocytes (green, cyan), and DAPI (blue), followed by quantification of percent BrdU + Sox9 + cells, normalized to the total number of $BrdU^+$ cells; n = 3 (Mock $Cre^−$), 5 (WNV $Cre^−$), 4 (Mock Cre^+), 7 (WNV Cre^+). E,F. Representative immunostaining of IL-1β (green), GFAP (red) and DAPI (blue) in CA3 region of the hippocampus of mock or WNV-infected Cre− or Cre+ animals at 25 (A) and 52 dpi (B), followed by quantification of GFAP + IL-1β + area, normalized to the total GFAP + area; n = 6 (Mock $Cre^−$ 25, WNV $Cre^−$ 25), 5 (Mock Cre^+ 25), 7 (WNV Cre^+ 25), 3 (Mock $Cre^−$ 52), 4 (WNV $Cre^−$ 52, Mock Cre^+ 52), 6 (WNV Cre^+ 52). Data were pooled from at least two independent experiments. Scale bars, 20 μm (B,D) 15 μm (E,F). Data represent the mean ± s.e.m. and were analyzed by two-way ANOVA and corrected for multiple comparisons.

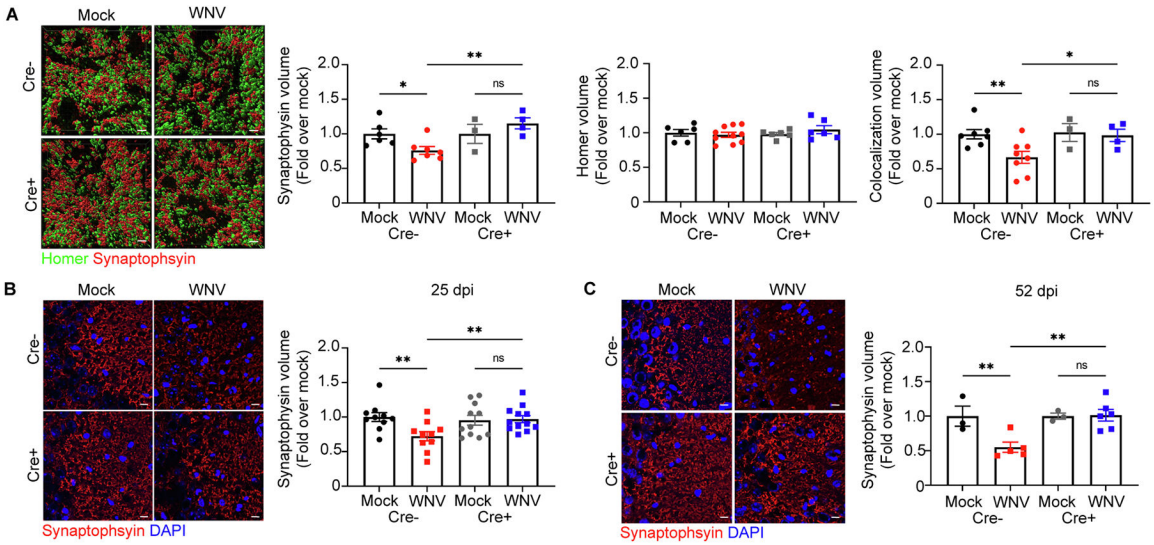

Fig. 4.

WNV-mediated alterations to synapse loss are prevented when IL-1R1 is specifically deleted from NSC. A. Representative 3D rendering of synapses in mock- or WNV-infected Cre− or CreERT + animals at 52 dpi, showing staining for homer (green), synaptophysin (red) and DAPI (blue), followed by quantification of synaptophysin+, homer+, and colocalization of synapse and homer volume in the CA3 of the hippocampus; n = 6–7 (Mock Cre^{-}), 7–10 (WNV Cre^{-}), 3–6 (Mock Cre^{+}), 4–6 (WNV Cre^{+}). B,C. Representative immunostaining of synapses in mock- or WNV-infected Cre− or Cre+ animals at 25 (A) and 52 dpi (B), showing staining for synaptophysin (red) and DAPI (blue), followed by quantification of synaptophysin-positive area in the CA3 of the hippocampus; n = 10 (Mock Cre^{-} 25, WNV Cre^{-} 25), 11 (Mock Cre^{+} 25), 12 (WNV Cre^{+} 25), 3 (Mock Cre^{-} 52, WNV Cre^{-}), 5 (WNV Cre^{-} 52), 6 (WNV Cre^{+} 52). Data were pooled from at least two independent experiments. Scale bars, 2 μm (A) or 10 μm (B,C). Data represent the mean ± s.e.m. and were analyzed by two-way ANOVA and corrected for multiple comparisons.

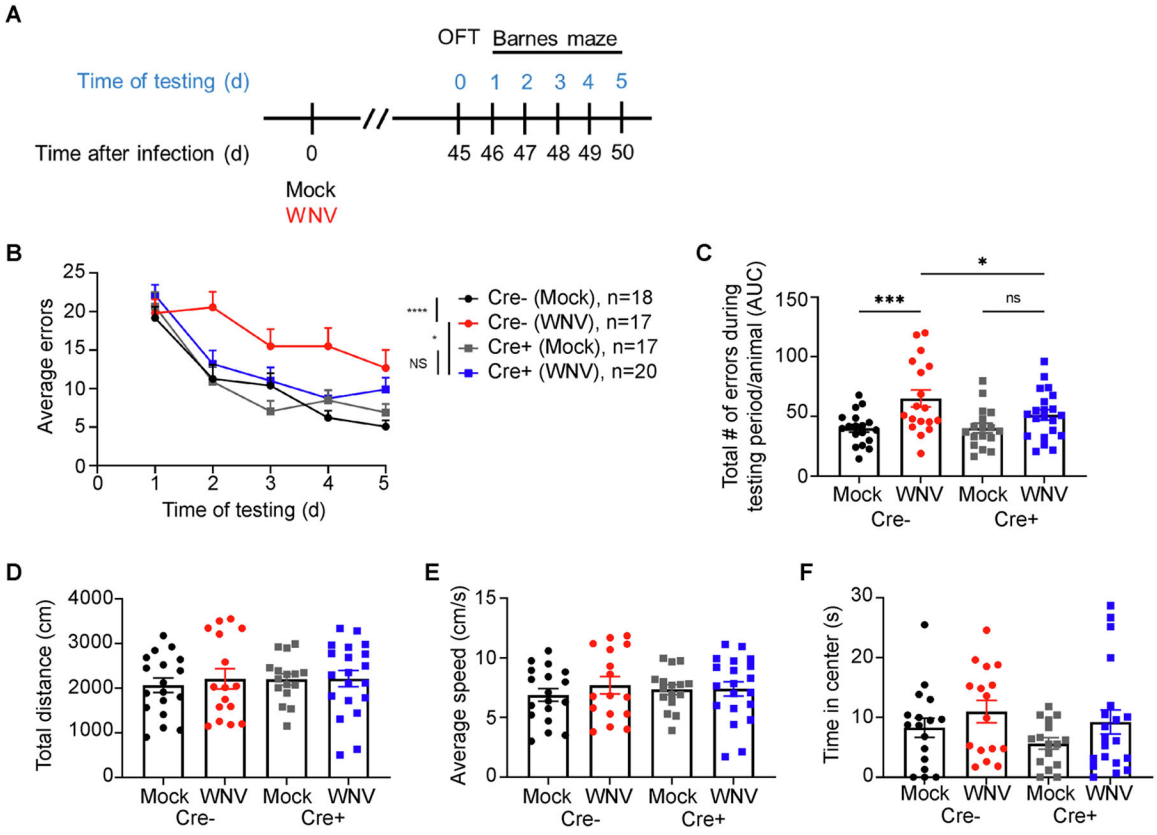

Fig. 5.

Loss of IL-1R1 signaling in NSC protects animals against spatial learning deficits 1 month after viral clearance. A. Experimental design: mice underwent behavioral testing beginning with OFT at 45 dpi, followed by 5 consecutive days of Barnes maze testing. B. Barnes maze performance, presented as average errors per trial of each group on each day of testing. C. Barnes maze error performance of mock- or WNV-E218A-infected Cre− or Cre+ animals, quantified as area under the curve for each individual animal within each group. d-f. OFT showing the total distance travelled (D), average speed (E) and total time spent in center (F) in 5 min of testing for each animal; n = 18 (Mock Cre^{-}), 17 (WNV Cre^{-}), 17 (Mock Cre^{+}), 20 (WNV Cre^{+}).

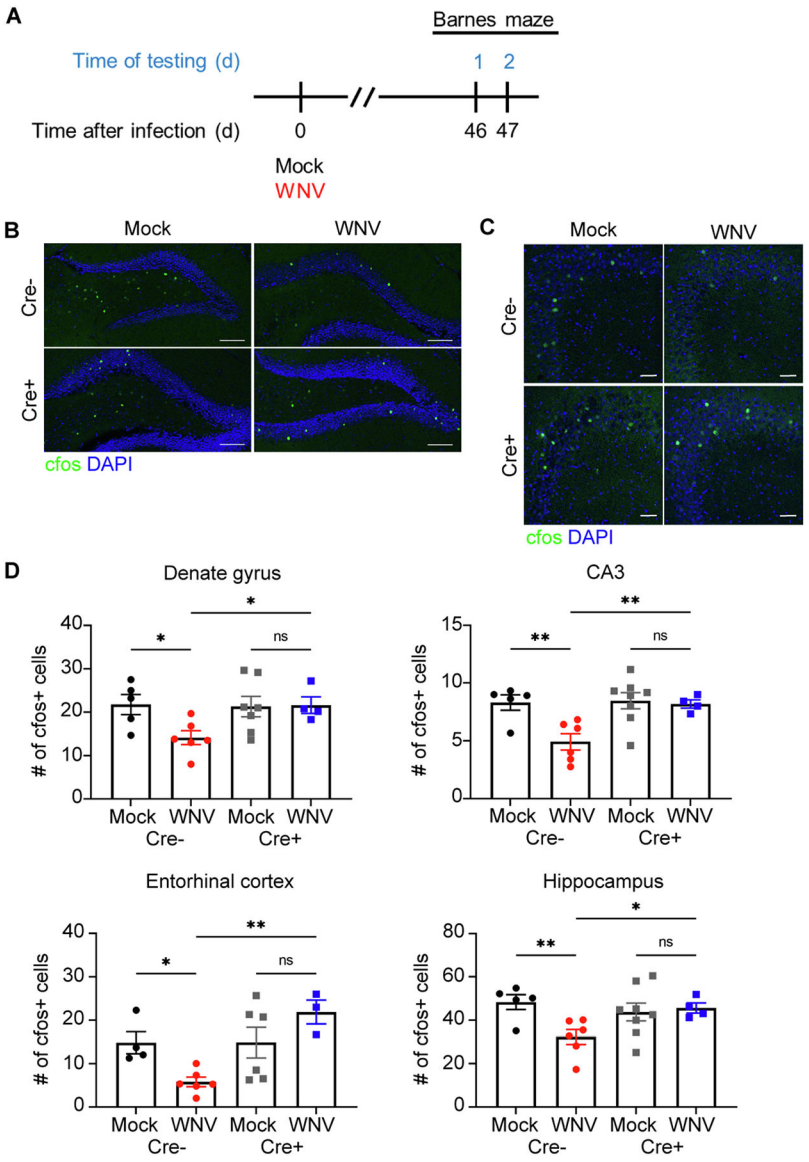

Fig. 6.

Hippocampal neural activity is disrupted in WNV-recovered animals, but loss of IL-1 signaling in NSC protects animals from these alterations. A. Experimental design: mice underwent behavioral testing at 46 dpi, followed by 2 consecutive days of Barnes maze testing. B,C. Microscopy of the dentate gyrus (B) and CA3 (C) region of mock or WNV-infected Cre− or Cre+ animals at 52 dpi, showing staining of CFOS (green) and DAPI (blue). D. Quantification of total CFOS + cells in the DG, CA3 region, entorhinal cortex and the entire hippocampal circuit. Data were pooled from at least two independent experiments; n = 4–5 (Mock Cre−), 5–6 (WNV Cre), 6–8 (Mock Cre^{+}), 3–4 (WNV Cre^{+}). Data represent the mean ± s.e.m. and analyzed by two-way ANOVA and corrected for multiple comparisons.

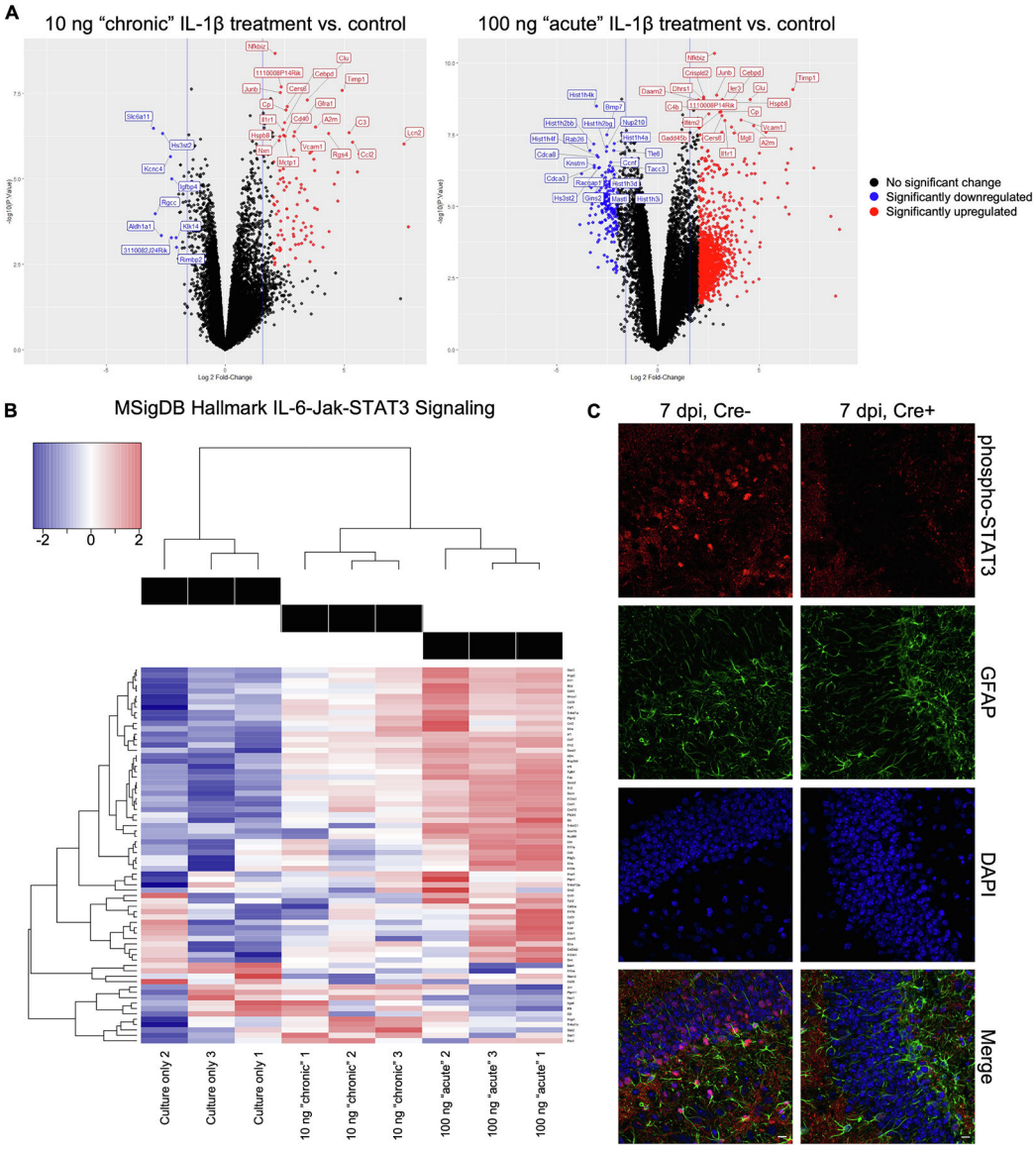

Fig. 7.

Transcriptional profile of IL-1β-treated adult primary neural stems cells suggests activation of signaling pathways associated with astrogenesis. A. Volcano plots of all genes statistically enriched or reduced in adult primary NSC treated in culture with murine IL-1β at 10 ng/mL for 7 days (chronic paradigm) or 100 ng/mL for 3 days (acute paradigm) compared to NSC cultured for 7 days without IL-1β. B. Heat map showing relative expression of significantly altered genes within the IL-6/Jak/STAT3 MSigDB Hallmark signaling pathway of non-treated and murine IL-1β-treated adult NSC. C. In vivo validation of differential phosphorylated STAT3 staining within the dentate gyrus of Cre+ and Cre− mice 7 dpi after WNV infection (pSTAT3, red; GFAP, green; DAPI, blue; scale, 10 um).